

# Harmonic Transfer-function-based Impedance Modelling of a Three-phase VSC for Asymmetric AC Grids Stability Analysis

Chen Zhang, Marta Molinas., *Member, IEEE*, Atle Rygg, Jing Lyu, Xu Cai

**Abstract**—Impedance modeling and stability analysis of a grid-VSC system under symmetric ac grids have been extensively discussed in the literature, where the  $dq$  domain impedances are usually adopted. As for asymmetric ac grids, impedance modeling is no longer straightforward in the  $dq$  domain due to the presence of negative sequence components, where the linearization will result in a linear-time-periodically-varying (LTPV) system, making the frequency-domain analysis intractable. One way to address this issue would be the harmonic-transfer-function (HTF) approach. Although this method is conceptually clear, its application to the stability analysis of an unbalanced grid-VSC system is still challenging and an effective model is missing here, therefore this paper aims to bridge this gap. First, the sequence impedances of an unbalanced grid-VSC system is modeled in the HTF framework. Then the HTFs are truncated into four-by-four matrices by exploiting the property of frequency couplings. Based on this, the equivalent source and load model for Nyquist-based analysis are established, and they are thoroughly verified by impedance measurements as well as the accuracy on stability analysis. Finally, several stability concerns of the unbalanced grid-VSC system, as well as the feasibility of symmetric models for asymmetric ac grid stability analysis are discussed and clarified.

**Index Terms**— converter, impedance, Nyquist-criterion, stability, time-varying, unbalance

## I. INTRODUCTION

VOLTAGE source converters (VSCs) have been widely utilized in the grid-integration of renewable energies, e.g. wind and solar [1], as well as the interconnection of asynchronous AC grids by means of high-voltage-dc (HVDC) technologies [2]. Recently, it has been identified that VSCs are susceptible to oscillate if the ac grid is weak [3], and they have been reported not only in wind farms [4] but also in photovoltaic power plants [5]. To study this, both the state-space-based ([6]-[8]) and the impedance-based methods can be applied. In this work, the impedance-based method is preferred, since most of the oscillations are caused by port-interactions,

for which the input-output characteristic is analyzed.

Analytical impedance modeling is a useful tool for stability assessment, as reported in [9] by X.F. Wang *et al.*, where different impedance modeling techniques are overviewed. Among them, the  $dq$ -impedance and the sequence-impedance are usually applied for stability analysis. Under symmetric ac grid conditions, a framework for the  $dq$  impedance modeling with constant-power-load (CPL) of VSCs and associated stability criteria was established in [10] by M. Belkhat. Afterward, more detailed impedances models including the phase-locked-loop (PLL) and other control loops are developed e.g. in [11] by B. Wen *et al* and in [12] by L. Harnfors *et al.*

Since the linear-time-invariant (LTI) property holds for the  $dq$ -domain models under symmetric three-phase conditions, corresponding impedances can be easily obtained by applying the Laplace transform on the linearized systems in  $dq$ -domain. If the VSC is directly linearized in the phase-domain (i.e.  $abc$  frame), the resulting model will be linear-time periodically varying (LTPV) because of the periodically time-varying operating points. Unlike the LTI system, translating an LTPV system into the frequency domain is no longer straightforward due to the presence of frequency couplings. One way to address this issue is to apply the harmonic linearization method of sequence components [13] (overviewed by J. Sun), by which the sequence impedances can be obtained, e.g. [14] and [15].

Interestingly, both the  $dq$  and the sequence impedance developed under three-phase symmetric conditions are two-by-two matrices, implying some bindings between them. This motivates the formation of other impedance modeling methods with different perspectives, e.g. a complex-vector-based ([16] and [17]), a modified-sequence-domain-based ([18] and [19]), and a phasor-based [20], from them the frequency-domain properties of VSCs can be better revealed, e.g. the mirror frequency coupling (MFC) [18] effect. It should be noted that a sound understanding of the frequency-domain properties is crucial and beneficial for impedance modeling, in particular, the model reductions. This resembles the importance of multi-

The work is supported by NTNU Energy (81617922), and the National Natural Science Foundation of China (51837007).

Chen Zhang, Department of Engineering Cybernetics, Norwegian University of Science and Technology, Trondheim, Norway (email: [chen.zhang@ntnu.no](mailto:chen.zhang@ntnu.no)).

Marta Molinas, Department of Engineering Cybernetics, Norwegian University of Science and Technology, Trondheim, Norway ([marta.molinas@ntnu.no](mailto:marta.molinas@ntnu.no)).

Atle Rygg, Department of Engineering Cybernetics, Norwegian University of Science and Technology, Trondheim, Norway (email: [atle.rygg@ntnu.no](mailto:atle.rygg@ntnu.no)).

Jing Lyu, Department of Electrical Engineering, Shanghai Jiao Tong University, Shanghai, China (email: [jinglv@sjtu.edu.cn](mailto:jinglv@sjtu.edu.cn)).

Xu Cai, Department of Electrical Engineering, Shanghai Jiao Tong University, Shanghai, China (email: [xucai@sjtu.edu.cn](mailto:xucai@sjtu.edu.cn)).

time-scale property to the power system dynamic modeling and analysis.

On the other hand, if the system is three-phase asymmetric, multiple frequency-couplings will present if it is perturbed. Therefore, a more general modeling method is required for mapping such LTPV systems into frequency-domain. In this respect, the harmonic-state-space (HSS) [21] and the harmonic-transfer-function (HTF) [22] method are applicable. The HSS method utilizes the so-called exponentially modulated

periodical (EMP) signals (e.g.  $e^{st} \cdot \sum_m U_m e^{jm\omega_1 t}$ ) [21] to achieve a state-space-like model, however, in the frequency domain, e.g.,  $s_n X_n = \sum_m A_{n-m} \cdot X_m + \sum_m B_{n-m} \cdot U_m$ ,  $X_n$  is the  $n$ th

Fourier coefficients of state-vector  $x$ . Due to this resemblance, a clarification of different state-space notations is necessary and presented in [23] by J. Kwon *et al.* Clearly, the larger the number of harmonics considered, the more accurate approximation of the HSS model will be. Applications of the HSS approach in harmonic modeling and resonance analysis of VSCs are studied in [23] and [24], it is shown that the HSS model is able to capture the harmonic dynamics up to switching frequency by choosing the number of harmonics sufficiently large. Whereas in [25] a relatively low harmonic-order is considered since the objective is to identify the control interactions between the modular-multilevel-converter (MMC) and the wind farm. On the other hand, although transforming an HSS model into transfer-functions is conceptually clear, it is difficult to achieve analytically due to the large model dimensions. In this regard, the HTF method can be an alternative since it is known as a generalized operator for directly mapping an LTPV system into the frequency domain. Due to this benefit, it is intuitive to applied to single-phase VSCs [26]. As for three-phase VSCs, since the three phases are tightly coupled through converter controls, the complexity is drastically increased even under symmetric conditions[27]. A numeric-based analysis as presented in [28] can be a choice, where the converter is viewed as a black/gray box. However, without the analytical model, insights of impedance characteristics and their effects on stability are hard to acquire.

In overall, the HTF approach lays a theoretical foundation for the frequency-domain modeling of LTPV systems. Although this method is conceptually clear, its application to the stability analysis of an unbalanced grid-VSC system is still challenging and a useful model is missing, therefore this paper aims to bridge this gap. First, in section II, an unbalanced grid-VSC system is modeled in the HTF framework and then transformed into the sequence-domain. Since the HTFs are of infinite dimensions, they cannot be used for analysis directly, an order-reduction (i.e. model truncation) by exploiting the property of frequency-couplings is presented in section III, where only the frequency components relevant to control dynamics are retained and extracted from the HTFs. Section IV further derives an equivalent source and load model for Nyquist-based stability analysis, its effectiveness is verified by frequency-sweeping as well as the accuracy in stability assessments.

Section V provides more impedance validations under grid-voltage asymmetry conditions. Also, the feasibility and performance of two types of symmetric impedance models on asymmetric ac grid stability analysis are discussed and clarified. Finally, section VI draws the main conclusions.

## II. SEQUENCE IMPEDANCE MODELING OF AN UNBALANCED GRID-VSC SYSTEM IN THE HTF FRAMEWORK

Fig. 1 presents a typical grid-tied VSC system, which is mainly composed of a three-phase and two-level VSC, a Thevenin equivalent ac grid and a step-up transformer. The dc voltage is assumed constant in this work, whereas the current control loop and the PLL will be modeled in detail.

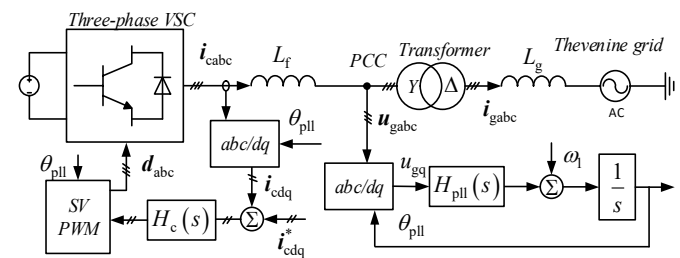


Fig. 1 A typical two-level and three-phase grid-tied VSC system

### A. A brief introduction of the HTF approach

The EMP signal is introduced to the HTF framework for properly capturing all the possible frequency couplings [21]:

$$u(t) = e^{st} \cdot \sum_m U_m e^{jm\omega_1 t} \quad (1)$$

where  $\omega_1$  is the fundamental frequency of the grid,  $s$  is the Laplace variable and  $U_m$  denotes the  $m$ th Fourier coefficient. If represents the signal  $U_m \cdot e^{st}$  as an implicit function of  $s$ , one may obtain its spectrum:  $U_m(s)$ . In this way, the EMP signal is related to a vector of spectra [22] as:

$$\mathbf{U}^{\text{htf}}(s) = [\dots U_{-1}(s) U_0(s) U_{+1}(s) \dots]^T \quad (2)$$

where  $\mathbf{U}^{\text{htf}}(s)$  denotes the vector of spectra, and the components within it, e.g.  $U_m(s)$  is regarded as the spectrum at  $m$ th frequency band (FB), or more illustratively speaking the information stored in the  $m$ th FB.

According to the HTF approach [22], an LTPV system in the frequency domain is formulated as:

$$\begin{bmatrix} \vdots \\ Y_{-1} \\ Y_0 \\ Y_{+1} \\ \vdots \end{bmatrix} = \underbrace{\begin{bmatrix} \ddots & & & & \vdots & & \ddots \\ & H_{(-1,-1)}(s) & H_{(-1,0)}(s) & H_{(-1,+1)}(s) & & & \\ \cdots & H_{(0,-1)}(s) & H_{(0,0)}(s) & H_{(0,+1)}(s) & \cdots & & \\ & H_{(+1,-1)}(s) & H_{(+1,0)}(s) & H_{(+1,+1)}(s) & & & \\ \ddots & & & & \vdots & & \ddots \end{bmatrix}}_{\mathbf{H}^{\text{htf}}(s)} \begin{bmatrix} \vdots \\ U_{-1} \\ U_0 \\ U_{+1} \\ \vdots \end{bmatrix} \quad (3)$$

where  $\mathbf{H}^{\text{htf}}(s)$  is referred to as the HTF. The component e.g.  $H_{(n,m)}(s)$  describes the coupling between input  $U_m(s)$  and



$$\begin{bmatrix} \mathbf{i}_{cd}^{\text{htf}}(s) \\ \mathbf{i}_{cq}^{\text{htf}}(s) \end{bmatrix} = \begin{bmatrix} \mathbf{I}_{cq0}^{\text{htf}} \\ -\mathbf{I}_{cd0}^{\text{htf}} \end{bmatrix} \Delta\theta_{\text{pll}}^{\text{htf}}(s) + \mathbf{T}_{\text{abc/dq}}^{\text{htf}} \begin{bmatrix} \mathbf{i}_{ca}^{\text{htf}}(s) \\ \mathbf{i}_{cb}^{\text{htf}}(s) \\ \mathbf{i}_{cc}^{\text{htf}}(s) \end{bmatrix} \quad (11)$$

where  $\mathbf{I}_{cd0}^{\text{htf}}$  is a Toeplitz matrix with nonzero elements:  $A_0 = I_{d0}$ ,  $A_2 = 0.5I_{n0}e^{j\phi}$ ,  $A_{-2} = 0.5I_{n0}e^{-j\phi}$ . Similarly,  $\mathbf{I}_{cq0}^{\text{htf}}$  is also a Toeplitz matrix with nonzero elements:  $A_0 = I_{q0}$ ,  $A_2 = 0.5jI_{n0}e^{j\phi}$ ,  $A_{-2} = -0.5jI_{n0}e^{-j\phi}$ .  $I_{n0}e^{j\phi}$  is the negative sequence current.

Similarly, the outputs of the current controller in HTF format can be derived:

$$\mathbf{T}_{\text{dq/abc}}^{\text{htf}} \begin{bmatrix} \mathbf{u}_{cd}^{\text{htf}}(s) \\ \mathbf{u}_{cq}^{\text{htf}}(s) \end{bmatrix} + \begin{bmatrix} \mathbf{U}_{ca0}^{\text{htf}} \\ \mathbf{U}_{cb0}^{\text{htf}} \\ \mathbf{U}_{cc0}^{\text{htf}} \end{bmatrix} \Delta\theta_{\text{pll}}^{\text{htf}}(s) = \begin{bmatrix} \mathbf{u}_{ca}^{\text{htf}}(s) \\ \mathbf{u}_{cb}^{\text{htf}}(s) \\ \mathbf{u}_{cc}^{\text{htf}}(s) \end{bmatrix} \quad (12)$$

Since this work focuses on the control interactions and associated stability issues, fast dynamics related to switching will be ignored, thus the output voltages of the converter are assumed equal to the controller outputs.

Substituting (11) and (12) into the current controller  $H_c(s)$  yields (15), where  $\mathbf{H}_c^{\text{htf}}(s)$  is frequency-shifted copies of  $H_c(s)$ .

Next, the voltage equation of the ac filter in HTF format is:

$$\begin{bmatrix} \mathbf{u}_{ca}^{\text{htf}}(s) \\ \mathbf{u}_{cb}^{\text{htf}}(s) \\ \mathbf{u}_{cc}^{\text{htf}}(s) \end{bmatrix} = \text{diag}(\mathbf{Z}_{fa}^{\text{htf}}, \mathbf{Z}_{fb}^{\text{htf}}, \mathbf{Z}_{fc}^{\text{htf}}) \begin{bmatrix} \mathbf{i}_{ca}^{\text{htf}}(s) \\ \mathbf{i}_{cb}^{\text{htf}}(s) \\ \mathbf{i}_{cc}^{\text{htf}}(s) \end{bmatrix} + \begin{bmatrix} \mathbf{u}_{ga}^{\text{htf}}(s) \\ \mathbf{u}_{gb}^{\text{htf}}(s) \\ \mathbf{u}_{gc}^{\text{htf}}(s) \end{bmatrix} \quad (13)$$

Substituting (10) and (13) into (15) finally yields the VSC-HTF admittance model in (16).

In (16), the Laplace variable  $s$  is omitted for brevity, and the condition  $\mathbf{Z}_{fa}^{\text{htf}} = \mathbf{Z}_{fb}^{\text{htf}} = \mathbf{Z}_{fc}^{\text{htf}} = \mathbf{Z}_f^{\text{htf}}$  is assumed in this study.

### C. HTF-modeling of the asymmetric ac grid

According to the above analysis, the Grid-HTF model is obtained in (14),

$$\mathbf{Z}_{\text{Grid}}^{\text{HTF}}(s) = \text{diag}(\mathbf{Z}_{ga}^{\text{htf}}(s), \mathbf{Z}_{gb}^{\text{htf}}(s), \mathbf{Z}_{gc}^{\text{htf}}(s)) \quad (14)$$

where the elements within the HTF e.g.  $\mathbf{Z}_{ga}^{\text{htf}}(s)$  are frequency-shifted copies of  $Z_{ga}(s) = sL_g + R_g$ .

In this study, the grid asymmetry is primarily interpreted as the grid impedance imbalance of three phases, hence  $Z_{ga}(s)$ ,  $Z_{gb}(s)$ ,  $Z_{gc}(s)$  are not necessarily the same.

### D. Symmetrical components of the HTF models

In power system analysis, symmetrical decomposition is a useful tool for analyzing an unbalanced three-phase system via three independent components [29], i.e. the positive sequence (PS), negative sequence (NS) and the zero sequence (ZS), where the ZS can be omitted if there are no paths for zero sequence currents flow.

The symmetrical decomposition is straightforward if applied to one set of three-phase periodical signals. As for the EMP signals, multiple harmonics should be decomposed consistently. This is fulfilled by decomposing the three-phase signals of each frequency bands one-by-one.

Taking the +1 FB (i.e.  $+f_1$ ) as an example, the three-phase variables in this FB are:  $U_{a(+1)}(s), U_{b(+1)}(s), U_{c(+1)}(s)$ .

According to the typical decomposition method, the symmetric components of this FB is [27]:

$$\begin{bmatrix} U_{P(+1)}(s) \\ U_{N(+1)}(s) \end{bmatrix} = \frac{1}{3} \begin{bmatrix} 1 & a & a^* \\ 1 & a^* & a \end{bmatrix} \begin{bmatrix} U_{a(+1)}(s) \\ U_{b(+1)}(s) \\ U_{c(+1)}(s) \end{bmatrix} \quad (17)$$

where  $a = e^{j\frac{2}{3}\pi}$ . It should be noted that the Laplace variable  $s$  if written explicitly is:  $s = j\omega, \omega > 0$ , where the frequency should be positive according to the definition.

Then, applying this method to all the FBs yields the symmetric components of an HTF model:

$$\begin{bmatrix} \mathbf{U}_P^{\text{htf}}(s) \\ \mathbf{U}_N^{\text{htf}}(s) \end{bmatrix} = \frac{1}{3} \begin{bmatrix} \mathbf{I} & \mathbf{a} & \mathbf{a}^* \\ \mathbf{I} & \mathbf{a}^* & \mathbf{a} \end{bmatrix} \begin{bmatrix} \mathbf{U}_a^{\text{htf}}(s) \\ \mathbf{U}_b^{\text{htf}}(s) \\ \mathbf{U}_c^{\text{htf}}(s) \end{bmatrix} \quad (18)$$

where  $\mathbf{I} = \text{diag}(\dots, 1, 1, 1, \dots)$ ,  $\mathbf{a} = \text{diag}(\dots, \mathbf{a}^*, \mathbf{a}, \mathbf{a}, \dots)$ .

Consequently, the VSC-HTF model i.e. (16) is transformed into sequence domain as

$$-\begin{bmatrix} \mathbf{i}_{cP}^{\text{htf}}(s) \\ \mathbf{i}_{cN}^{\text{htf}}(s) \end{bmatrix} = \frac{1}{3} \begin{bmatrix} \mathbf{I} & \mathbf{a} & \mathbf{a}^* \\ \mathbf{I} & \mathbf{a}^* & \mathbf{a} \end{bmatrix} \mathbf{Y}_{\text{VSC}}^{\text{HTF}}(s) \begin{bmatrix} \mathbf{I} & \mathbf{I} \\ \mathbf{a}^* & \mathbf{a} \\ \mathbf{a} & \mathbf{a}^* \end{bmatrix} \begin{bmatrix} \mathbf{u}_{gP}^{\text{htf}}(s) \\ \mathbf{u}_{gN}^{\text{htf}}(s) \end{bmatrix} \quad (19)$$

Likewise, the sequence domain Grid-HTF model is obtained from (14) as:

$$\begin{bmatrix} \mathbf{u}_{gP}^{\text{htf}}(s) \\ \mathbf{u}_{gN}^{\text{htf}}(s) \end{bmatrix} = \frac{1}{3} \begin{bmatrix} \mathbf{I} & \mathbf{a} & \mathbf{a}^* \\ \mathbf{I} & \mathbf{a}^* & \mathbf{a} \end{bmatrix} \mathbf{Z}_{\text{Grid}}^{\text{HTF}}(s) \begin{bmatrix} \mathbf{I} & \mathbf{I} \\ \mathbf{a}^* & \mathbf{a} \\ \mathbf{a} & \mathbf{a}^* \end{bmatrix} \begin{bmatrix} \mathbf{i}_{gP}^{\text{htf}}(s) \\ \mathbf{i}_{gN}^{\text{htf}}(s) \end{bmatrix} \quad (20)$$

$$\begin{bmatrix} \mathbf{u}_{ca}^{\text{htf}}(s) \\ \mathbf{u}_{cb}^{\text{htf}}(s) \\ \mathbf{u}_{cc}^{\text{htf}}(s) \end{bmatrix} = \begin{bmatrix} \mathbf{U}_{ca0}^{\text{htf}} \\ \mathbf{U}_{cb0}^{\text{htf}} \\ \mathbf{U}_{cc0}^{\text{htf}} \end{bmatrix} - \mathbf{T}_{\text{dq/abc}}^{\text{htf}} \begin{bmatrix} \mathbf{H}_c^{\text{htf}}(s) \mathbf{I}_{cq0}^{\text{htf}} \\ -\mathbf{H}_c^{\text{htf}}(s) \mathbf{I}_{cd0}^{\text{htf}} \end{bmatrix} \Delta\theta_{\text{pll}}^{\text{htf}}(s) - \mathbf{T}_{\text{dq/abc}}^{\text{htf}} \begin{bmatrix} \mathbf{H}_c^{\text{htf}}(s) & 0 \\ 0 & \mathbf{H}_c^{\text{htf}}(s) \end{bmatrix} \mathbf{T}_{\text{abc/dq}}^{\text{htf}} \begin{bmatrix} \mathbf{i}_{ca}^{\text{htf}}(s) \\ \mathbf{i}_{cb}^{\text{htf}}(s) \\ \mathbf{i}_{cc}^{\text{htf}}(s) \end{bmatrix} \quad (15)$$

$$\mathbf{Y}_{\text{VSC}}^{\text{HTF}}(s) = \left( \text{diag}(\mathbf{Z}_{fa}^{\text{htf}}, \mathbf{Z}_{fb}^{\text{htf}}, \mathbf{Z}_{fc}^{\text{htf}}) + \mathbf{T}_{\text{dq/abc}}^{\text{htf}} \begin{bmatrix} \mathbf{H}_c^{\text{htf}} & 0 \\ 0 & \mathbf{H}_c^{\text{htf}} \end{bmatrix} \mathbf{T}_{\text{abc/dq}}^{\text{htf}} \right)^{-1} \left\{ \mathbf{I} + \left( \mathbf{T}_{\text{dq/abc}}^{\text{htf}} \begin{bmatrix} \mathbf{H}_c^{\text{htf}} \mathbf{I}_{cq0}^{\text{htf}} \\ -\mathbf{H}_c^{\text{htf}} \mathbf{I}_{cd0}^{\text{htf}} \end{bmatrix} - \begin{bmatrix} \mathbf{U}_{ca0}^{\text{htf}} \\ \mathbf{U}_{cb0}^{\text{htf}} \\ \mathbf{U}_{cc0}^{\text{htf}} \end{bmatrix} \mathbf{T}_{\text{pll}}^{\text{htf}} \cdot \mathbf{T}_{\text{sin}}^{\text{htf}} \right) \right\} \quad (16)$$

where the inputs and outputs are still vectors of spectra, e.g.

$$\mathbf{i}_{gP}^{\text{htf}} = [\dots, i_{P(-)}(s), i_{P(0)}(s), i_{P(+)}(s), \dots]^T, \quad \text{and}$$

$$\mathbf{i}_{gN}^{\text{htf}} = [\dots, i_{N(-)}(s), i_{N(0)}(s), i_{N(+)}(s), \dots]^T.$$

So far, the HTF model of an unbalanced grid-VSC system is achieved, where the HTFs are infinitely dimensional matrices characterizing all the possible frequency couplings. Therefore, they cannot be used for analysis directly, and proper model truncation is required. Since this work aims at acquiring an analytical model for control-related stability analysis, this implies that only a few frequency components of the HTFs are crucial for this study. To this consideration, a method for truncating the HTFs will be shown in the next section.

### III. PROPERTIES OF THE FREQUENCY COUPLINGS AND FORMULATION OF THE FIRST COUPLING CYCLE MODEL

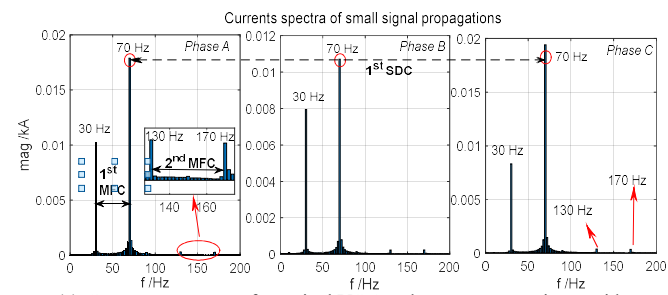
#### A. Properties of the frequency couplings relevant to controls

In a previous analysis [18], the MFC effect of the VSC is identified, i.e. if a positive sequence perturbation at a frequency e.g.  $f_p + f_1$ , is applied, the current responses of the VSC will show up two frequency components, one is  $f_p + f_1$  and the other is  $-f_p + f_1$ , or illustratively speaking  $\pm f_p + f_1$  at +1 FB (see Fig. 2 (a), the 1<sup>st</sup> MFC). This phenomenon is caused by the unequal regulation effects of VSC controls on the  $d$  and  $q$  axis variables, e.g. the PLL effect. Further, since the grid-VSC forms a closed-loop system, the outputs of the VSC are the inputs of the grid. As a result, if the grid impedance is three-phase *symmetric*, then the voltage responses (as vectors) will be of the same frequency and direction as the perturbation inputs, i.e.  $\pm f_p + f_1$ . Therefore, the number of frequency-couplings is finite for three-phase symmetric cases, which is two. This also explains why the impedance models of VSCs (three-phase and two-level) regardless of domains are two-by-two matrices under symmetrical grids.

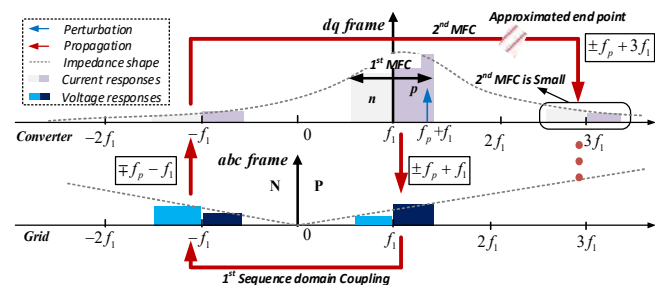
However, if the grid-impedance is three-phase *asymmetric*, it is known that the output voltages across the three-phase impedances will be unbalanced even if the input currents are balanced. In sequence domain, this feature is equivalent to the change of input directions, e.g. a positive sequence current flowing into the unbalanced the grid will additionally produce a negative sequence voltage. Based on this property, the inputs of the grid at  $\pm f_p + f_1$  (i.e. the 1<sup>st</sup> MFC current-outputs of the VSC) will result in two new responses at  $\mp f_p - f_1$ . This process, in this work, is denoted as the *sequence domain coupling* (SDC) effect of the grid. As shown in Fig. 2 (a), the magnitudes of three-phase currents (e.g. at 70Hz) are no longer equal, indicating the existence of SDC (in Fig. 2 (a), the steady-state operating points are removed from the spectra to acquire a clear illustration of the small-signal propagations).

After this *first coupling cycle* (FCC, composed of 1<sup>st</sup> MFC and 1<sup>st</sup> SDC) completes, the VSC will initiate the 2<sup>nd</sup> MFC, creating new responses at  $\pm f_p + 3f_1$  (see Fig. 2 (a), the 2<sup>nd</sup> MFC, and a more illustration in Fig. 2 (b)). Clearly, this process

resembles a “chain reaction” that starts from the injection at  $f_p + f_1$  but never ends, one may refer to [30] for a more general discussion on the infinite many frequency couplings.



(a) Current responses of a typical VSC under an asymmetric ac grid



(b) Illustration of the frequency coupling and the first coupling cycle

Fig. 2 A qualitative study of the frequency coupling properties with the presence of grid asymmetry (In (a), a fast VSC control is employed for illustration, and the phase C impedance is 10% of phase A and B)

Since the MFC effects are primarily dependent on the VSC controls, which are bandlimited signals in general, hence this “chain reaction” can be approximately ended at a point where the MFC effects become weak and negligible. In this work, the 2<sup>nd</sup> MFC is chosen as the “end point” due to its negligible responses, see the comparison of 1<sup>st</sup> and 2<sup>nd</sup> MFC effects in Fig. 2 (a).

In summary, only the dynamics relevant to the FCC is of most concern and should be modeled in detail. Next, the HTFs will be truncated into lower dimensions based on this criterion.

#### B. Derivation of the VSC and the grid FCC model

According to the above analysis, there are only four frequency components involved in the process of FCC, thereby a four-by-four matrix is expected for modeling their dynamics and interactions. This is fulfilled by extracting relevant frequency components from the HTF models.

##### 1) Derivation of the VSC-FCC model

The VSC-FCC model (21) is developed by extracting the frequency components  $\mp f_p \pm f_1$  from its HTF model (19), the transfer-functions of (21) are listed in Table I. It should be noted that the symmetry condition:  $G^*(-s) = G(s)$  may not hold generally if the transfer-functions (e.g.  $a(s)$ ) are of complex-valued coefficients.

Also, it is worth clarifying that, a straightforward way for representing the components  $\pm f_p + f_1$  is to adopt the complex-vector notation as presented in [16]. This means the positive and negative sequence component are unified by defining the

Table I Transfer functions of the VSC-FCC model

$a(s) = \frac{1 - \frac{T_{pll}(s)}{2}(U_{c0}^* + I_{c0}^* H_c(s))}{Z_f(s - j\omega_1) + H_c(s)}$	$b(s) = \frac{T_{pll}(s)}{2}(U_{c0} + I_{c0} H_c(s))}{Z_f(s + j\omega_1) + H_c(s)}$	$d(s) = \frac{T_{pll}(s)}{2}(U_{cn0}^* + I_{cn0}^* H_c(s - 2j\omega_1))}{Z_f(s - j\omega_1) + H_c(s - 2j\omega_1)}$
$c(s) = \frac{T_{pll}(s - 2j\omega_1)}{2}(U_{cn0} + I_{cn0} H_c(s))}{Z_f(s - j\omega_1) + H_c(s)}$	$e(s) = \frac{1 - \frac{T_{pll}(s - 2j\omega_1)}{2}(U_{c0} + I_{c0} H_c(s - 2j\omega_1))}{Z_f(s - j\omega_1) + H_c(s - 2j\omega_1)}$	

Laplace variable  $s$  of a function can be either positive or negative, e.g.  $i_c(s + j\omega_1), s = \pm j\omega_p$ . However, by definition, the employed symmetrical decomposition method regards the variable  $s$  as positive. Hence, the complex-vector notation has to be separated by  $i_{cp}(j\omega_p + j\omega_1)$  and  $i_{cp}(j\omega_p - j\omega_1)$ , where  $i_{cp}(j\omega_p - j\omega_1)$  is the conjugation of  $i_{cp}(-j\omega_p + j\omega_1)$ . Similarly,  $i_{cn}(s - j\omega_1)$  and  $i_{cn}(s + j\omega_1)$  are obtained from the complex-vector  $i_c(s - j\omega_1)$  with  $s = \mp j\omega_p$ .

Based on this notation, the submatrix  $\mathbf{Y}_{cPP}^{htf}$  of the VSC-FCC model is correlated to the *modified* sequence domain VSC model in [18], where  $a^*(-s) \rightarrow Y_{pp}(s)$ ,  $a(s) \rightarrow Y_{nn}(s)$ ,  $b(s) \rightarrow Y_{pn}(s)$ ,  $b^*(-s) \rightarrow Y_{np}(s)$  (the lower case “pn” denotes the frequency notation of the modified sequence domain, where the base-frequency of complex vectors is  $+\omega_1$ ). In turn, the FCC model can be regarded as an extension to the typical (modified) sequence domain model.

### 2) Derivation of the Grid-FCC model

Similar to the derivation of the VSC-FCC model, the Grid-FCC model is developed in (22) by extracting the same frequency components from (20).

In (22),  $m(s) = Z_g(s - j\omega_1)$ , where the three-phase asymmetry is introduced as the imbalance among grid impedances, i.e.  $Z_{ga} = Z_{gb} \neq Z_{gc}$ . Meanwhile, the *asymmetry factor* is defined as:  $k_z = Z_{gc} / Z_{ga}$ . Given by this definition,  $k_0 = 1 + \sqrt{3}j$ , leaving  $k_1, k_2$  are two additional constants related to  $k_z$ , see Table II for the values of grid asymmetry under this definition.

Table II Parameters of  $k_1$  and  $k_2$  with different values of  $k_z$

Phase C asymmetry	$k_1$	$k_2$
$k_z = 0.1$	7/10	3/20
$k_z = 0.5$	5/6	1/12
$k_z = 1$ (symmetric case)	1	0
$k_z = 2$	4/3	1/6
$k_z = 10$	4	3/2

### 3) Characteristics and interpretations of the VSC-FCC and the Grid-FCC model

This section aims to acquire a qualitative understanding of the FCC models regarding the characteristics and interpretations of the components. For better illustration, the magnitude responses of the VSC- and Grid-FCC model are plotted in Fig. 3, the main parameters are listed in Table III.

Table III Main parameters of the grid-VSC system

Name	value	Name	value
$S_{base}$	2 MW	$L_g$	0.25 p.u (SCR = 4)
$U_{base}$	690 V	$k_1$	5/6
$H_c$	200 Hz	$k_2$	1/12
$H_{pll}$	50 Hz	$L_f$	0.1 p.u

It is seen that the respective off-diagonal submatrices of the VSC-FCC and the Grid-FCC model are evident, indicating the existence of SDC effect. It is easily accepted that the grid is sequence-domain coupled since the three-phase impedance of this study is imbalanced, and the coupling strength can be qualitatively evaluated from the magnitudes of  $|\mathbf{Z}_{gPN}^{htf}(s)|, |\mathbf{Z}_{cNP}^{htf}(s)|$ . As for the VSC, one may argue that the SDC should not present since it is assumed three-phase symmetric in this study. In fact,  $\mathbf{Y}_{cPN}^{htf}(s), \mathbf{Y}_{cNP}^{htf}(s)$  are correlated with the negative sequence components of steady states (see the models in Table I, e.g.  $c(s)$  and  $d(s)$ ), which are existent due to the asymmetric ac grid. If the grid is symmetric,

$$\begin{aligned}
 \begin{bmatrix} i_{cP}(s - j\omega_1) \\ i_{cP}(s + j\omega_1) \\ i_{cN}(s - j\omega_1) \\ i_{cN}(s + j\omega_1) \end{bmatrix} &= \begin{bmatrix} \mathbf{Y}_{cPP}^{htf} = \begin{bmatrix} a(s) & b^*(-s) \\ b(s) & a^*(-s) \end{bmatrix} \\ \mathbf{Y}_{cNP}^{htf}(s) = \begin{bmatrix} d(s) & -d(s) \\ -d^*(-s) & d^*(-s) \end{bmatrix} \end{bmatrix} \begin{bmatrix} \mathbf{Y}_{cPN}^{htf}(s) = \begin{bmatrix} c(s) & 0 \\ 0 & c^*(-s) \end{bmatrix} \\ \mathbf{Y}_{cNN}^{htf}(s) = \begin{bmatrix} e(s) & 0 \\ 0 & e^*(-s) \end{bmatrix} \end{bmatrix} \begin{bmatrix} u_{gP}(s - j\omega_1) \\ u_{gP}(s + j\omega_1) \\ u_{gN}(s - j\omega_1) \\ u_{gN}(s + j\omega_1) \end{bmatrix} \quad (21)
 \end{aligned}$$

$$\begin{aligned}
 \begin{bmatrix} u_{gP}(s - j\omega_1) \\ u_{gP}(s + j\omega_1) \\ u_{gN}(s - j\omega_1) \\ u_{gN}(s + j\omega_1) \end{bmatrix} &= \begin{bmatrix} \mathbf{Z}_{gPP}^{htf} = k_1 \begin{bmatrix} m(s) & 0 \\ 0 & m^*(-s) \end{bmatrix} \\ \mathbf{Z}_{gNP}^{htf} = k_2 \begin{bmatrix} k_0 m(s) & 0 \\ 0 & k_0 m^*(-s) \end{bmatrix} \end{bmatrix} \begin{bmatrix} \mathbf{Z}_{gPN}^{htf} = k_2 \begin{bmatrix} k_0 m(s) & 0 \\ 0 & k_0 m^*(-s) \end{bmatrix} \\ \mathbf{Z}_{gNN}^{htf} = k_1 \begin{bmatrix} m(s) & 0 \\ 0 & m^*(-s) \end{bmatrix} \end{bmatrix} \begin{bmatrix} i_{gP}(s - j\omega_1) \\ i_{gP}(s + j\omega_1) \\ i_{gN}(s - j\omega_1) \\ i_{gN}(s + j\omega_1) \end{bmatrix} \quad (22)
 \end{aligned}$$

> REPLACE THIS LINE WITH YOUR PAPER IDENTIFICATION NUMBER (DOUBLE-CLICK HERE TO EDIT) < 7

then  $\mathbf{Y}_{cPN}^{htf}(s), \mathbf{Y}_{cNP}^{htf}(s)$  will not exist. Therefore, the SDC effect of the VSC, in this analysis, could be roughly interpreted as the consequence of grid asymmetry.

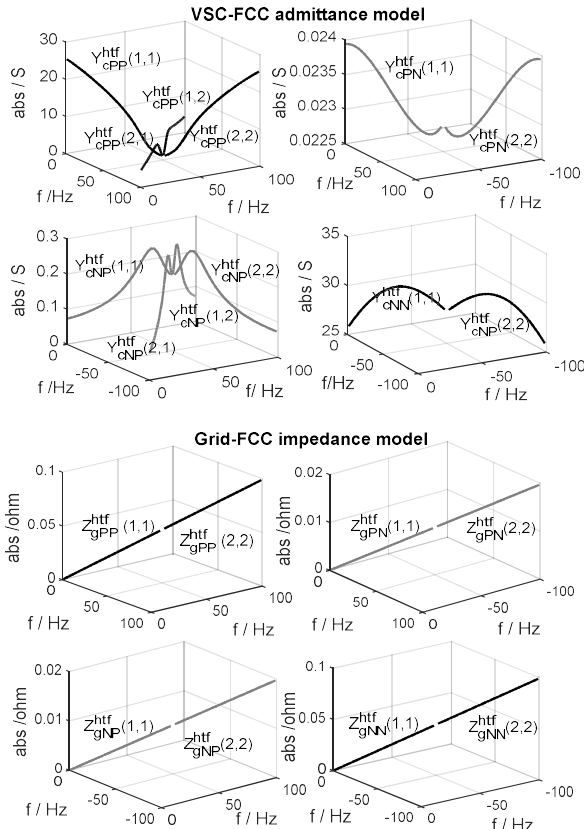


Fig. 3 Magnitude responses of the VSC- and the Grid-FCC models

Furthermore, it is seen that the off-diagonals of the diagonal submatrices i.e.,  $\mathbf{Y}_{cPP}^{htf}(s), \mathbf{Y}_{cNN}^{htf}(s)$ , are related with the MFC effect of VSC. In which, the off-diagonals of  $\mathbf{Y}_{cPP}^{htf}(s)$  is already well-understood, i.e. typical MFC effect under symmetric grid conditions [18]. Also, notice that the off-diagonals of  $\mathbf{Y}_{cNN}^{htf}(s)$  are null, this is because the frequency components:  $\mp f_p - f_1$  are mirror-frequency coupled with components:  $-(\mp f_p - f_1) + 2f_1 = \pm f_p + 3f_1$ , which are outside the scope of the FCC (i.e. 2<sup>nd</sup> MFC in Fig. 2 (b)).

#### IV. EQUIVALENT SOURCE AND LOAD MODEL FOR THE NYQUIST-BASED STABILITY ANALYSIS

As the Grid-FCC and the VSC-FCC model are four-by-four matrices, impedance verification can be lengthy since four sets of data are required for each measurement. Considering the modeling purpose is for stability analysis, which is essentially a closed-loop issue that can be studied by the impedance-ratio of a source and load system [31]. A previous study in [19] has explored in this respect and proposed a method to convert the two-by-two matrix model into SISO equivalents in the (modified) sequence domain, which drastically reduced the complexity in analysis and verification.

According to that analysis, if the grid-VSC system is perturbed by an independent perturbation of positive sequence (see Fig. 4 (a),  $u_{ptb}$ ), then the SISO-based equivalent source and load models can be found as:  $Z_{cq}^S(s)i_p^c = u_p^g$  and  $-i_p^c = Y_{eq}^L(s)u_p^c$ . Moreover, it is identified that the *marginally stable/unstable conditions* of the SISO-based and the two-by-two matrix-based model are identical, because of the condition  $\det(-1 + Z_{cq}^S Y_{eq}^L)_{SISO} = \det(-I_{2 \times 2} + Z_{pn}^{Grid} Y_{pn}^{VSC})_{MIMO} = 0$  holds simultaneously. This condition conveys a fact that the SISO-based models, though with lower dimensions, have the same accuracy as the MIMO models in terms of stability. Therefore, this method will be applied to the FCC model to find its lower dimensional source and load equivalents for stability analysis.

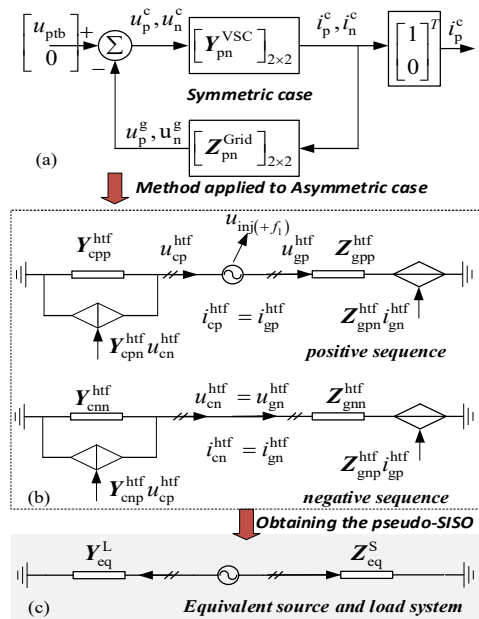


Fig. 4 Derivation of the equivalent source and load circuit

#### A. Derivation of the equivalent source and load models from the FCC model

In this analysis, a similar closed-loop system as Fig. 4 (a) can be constructed, except that the grid and VSC models (two-by-two matrices) are replaced with corresponding FCC models. As a result, the positive and negative sequence circuit based on the FCC models can be drawn as Fig. 4 (b), where the independent perturbations of  $+f_1$  FB are applied.

Under this configuration, the equivalent source and load models (illustratively, the pseudo-SISO model due to the concept and method) can be derived similarly as [19] by solving the coupled sequence circuits. After some circuit operations, the equivalent load model, defined as  $-i_{cp}^{htf}(s) = Y_{eq}^L(s) \cdot u_{cp}^{htf}(s)$  is obtained in (23), where  $u_{cp}^{htf} = [u_{cP(-)}(s), u_{cP(+)}(s)]^T$ ,

$$i_{cp}^{htf} = [i_{cP(-)}(s) \quad i_{cP(+)}(s)]^T.$$

$$\mathbf{Y}_{eq}^L(s) = \left[ \mathbf{I}_{2 \times 2} + \mathbf{Y}_{cPN}^{htf} \left( \mathbf{I}_{2 \times 2} + \mathbf{Z}_{gNN}^{htf} \mathbf{Y}_{cNN}^{htf} \right)^{-1} \mathbf{Z}_{gPN}^{htf} \right]^{-1} \cdot \left[ \mathbf{Y}_{cPP}^{htf} - \mathbf{Y}_{cPN}^{htf} \left( \mathbf{I}_{2 \times 2} + \mathbf{Z}_{gNN}^{htf} \mathbf{Y}_{cNN}^{htf} \right)^{-1} \mathbf{Z}_{gNP}^{htf} \mathbf{Y}_{cNP}^{htf} \right] \quad (23)$$

$$\mathbf{Z}_{eq}^S(s) = \mathbf{Z}_{gPP}^{htf} - \mathbf{Z}_{gPN}^{htf} \left( \mathbf{I}_{2 \times 2} + \left( \mathbf{Y}_{cNN}^{htf} - \mathbf{Y}_{cNP}^{htf} \left( \mathbf{Y}_{cPP}^{htf} \right)^{-1} \mathbf{Y}_{cPN}^{htf} \right) \mathbf{Z}_{gNN}^{htf} \right)^{-1} \left[ \left( \mathbf{Y}_{cNN}^{htf} - \mathbf{Y}_{cNP}^{htf} \left( \mathbf{Y}_{cPP}^{htf} \right)^{-1} \mathbf{Y}_{cPN}^{htf} \right) \mathbf{Z}_{gNP}^{htf} - \mathbf{Y}_{cNP}^{htf} \left( \mathbf{Y}_{cPP}^{htf} \right)^{-1} \right] \quad (24)$$

Likewise, the equivalent source model defined as:  $\mathbf{u}_{gp}^{htf}(s) = \mathbf{Z}_{eq}^L(s) \cdot \mathbf{i}_{gp}^{htf}(s)$  is obtained in (24), where

$$\mathbf{i}_{gp}^{htf} = \left[ i_{gp(-)}^{htf}(s), i_{gp(+)}^{htf}(s) \right]^T, \mathbf{u}_{gp}^{htf} = \left[ u_{gp(-)}^{htf}(s), u_{gp(+)}^{htf}(s) \right]^T.$$

Finally, an equivalent source and load system (i.e. the pseudo-SISO model) is established in Fig. 4 (c), based on which the impedance validation and the Nyquist-based stability analysis will be performed. Notice again, although the equivalent models are of lower dimensions, the accuracy on

stability analysis will not be sacrificed due to the identical marginal stability condition.

### B. Model verification by measured frequency responses

In this section,  $\mathbf{Y}_{eq}^L(s)$  and  $\mathbf{Z}_{eq}^S(s)$  will be verified through frequency-scanning. Benefit from the low model dimension, only two sets of data are required for the impedance measurement of a single frequency point, and the main process is shown in see Fig. 6, in general, it resembles the  $dq$  or the modified sequence impedance measurements.

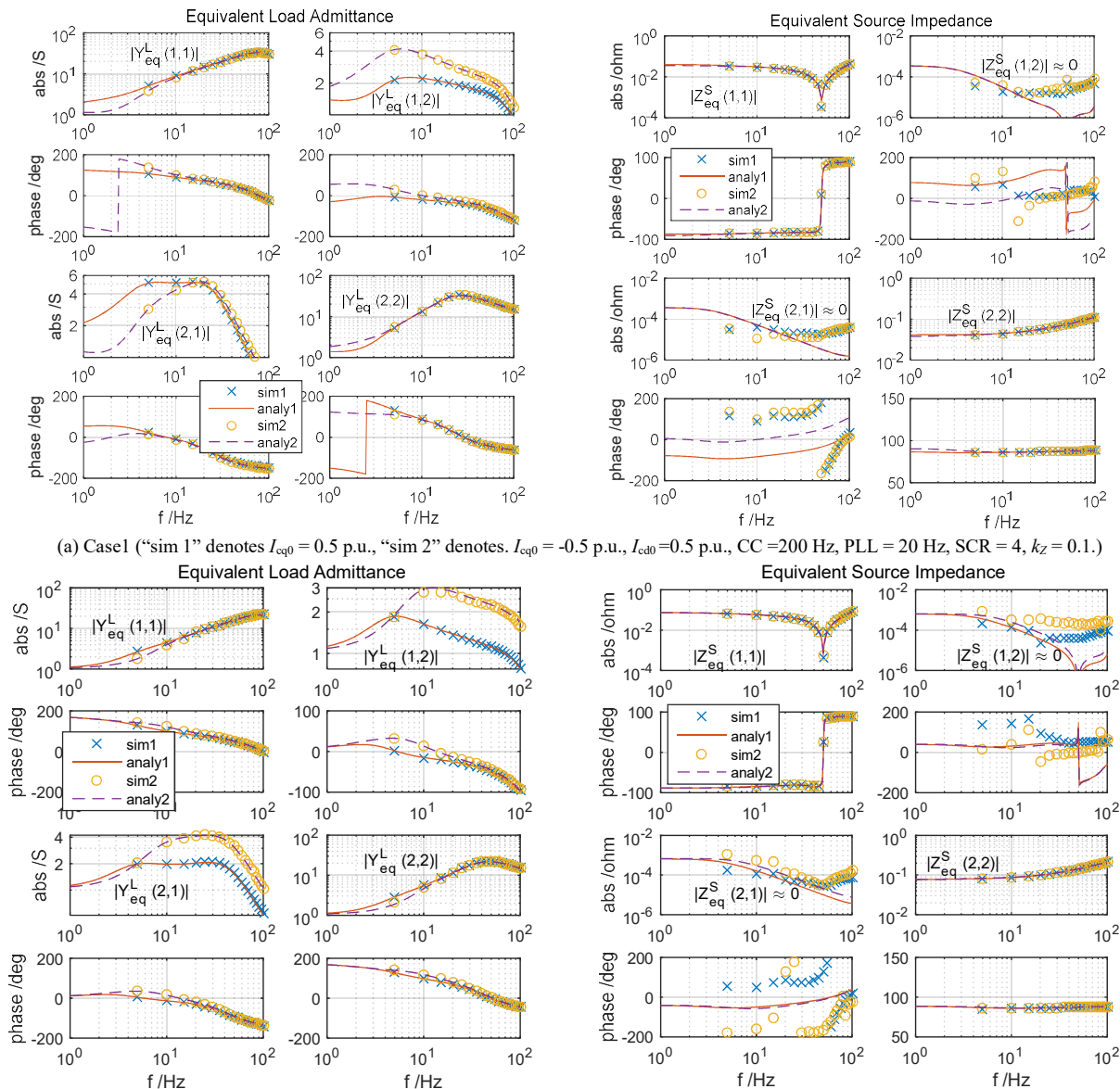


Fig. 5 Impedance model validation under various system configurations



It should be noted that, due to the significant nonlinearities, analytical calculation of the system's steady states is intractable, thereby simulation data are employed in this analysis. Also, under asymmetric cases, control parameters will greatly affect the operating points, which means they are not valid for a wide span of parameter changes. Hence, for more accurate impedance validation and stability analysis, it is suggested to update the operating points once a large change of control parameters is registered.

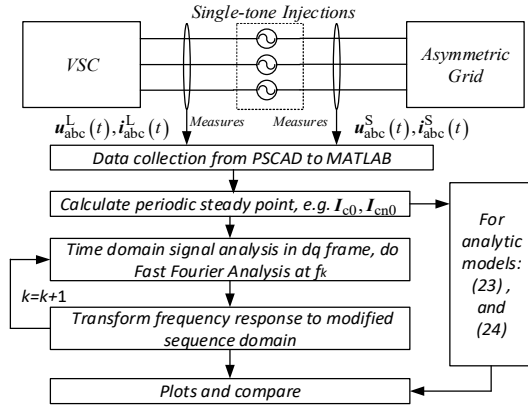


Fig. 6 A flow chart for impedance measurement in simulation

In Fig. 5 (a) Case 1, two types of reactive current injections are considered to address the effects of operating points. Overall,  $Y_{eq}^L(s)$  is consistent with measurements, whereas  $Z_{eq}^S(s)$  only achieves the consistency on the diagonals. The discrepancy appeared at the off-diagonals could be the consequence of either the model truncation or the un-modeled high-frequency components. However, overall, they are small compared to the diagonals, thereby negligible effects on stability is anticipated. This remark is qualitatively justified by inspecting the eigen-loci, for which the following equation:

$$\lambda^2 - (Z_{eq(2,2)}^S + Z_{eq(1,1)}^S)\lambda + Z_{eq(2,2)}^S Z_{eq(1,1)}^S - Z_{eq(1,2)}^S Z_{eq(2,1)}^S = 0 \quad (25)$$

is solved. Due to the small amplitudes of  $Z_{eq(1,2)}^S$  and  $Z_{eq(2,1)}^S$ , the last term in the characteristic equation is second-order smaller, i.e.,  $|Z_{eq(1,2)}^S Z_{eq(2,1)}^S| \ll |Z_{eq(2,2)}^S Z_{eq(1,1)}^S|$  holds. Therefore, the dominant characteristic of the equivalent source is determined by the diagonals. A further study on the stability effects will be shown in the next section.

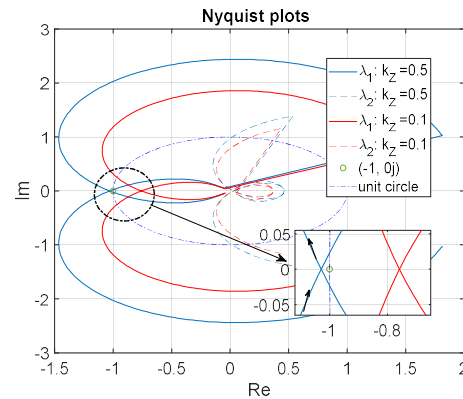
Next, Fig. 5 (b) Case 2 further considers two sets of PLL bandwidths to show the control effects. It is observed that the analytical models are consistent with the measurements except for some discrepancies on the off-diagonals of the equivalent source model. As addressed before, since these discrepancies remain small, the former justification on stability effects is still valid. On the other hand, from the load model, it is also seen that the larger the PLL bandwidth the greater the MFC effect due to the enlarged magnitudes of off-diagonals.

### C. Nyquist-based stability analysis and validation

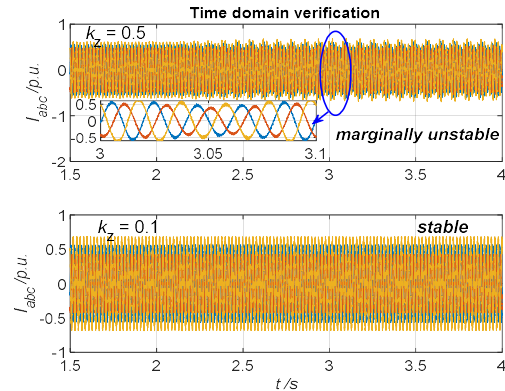
This section will perform the validation and analysis in terms of Nyquist-based stability. For which, the eigen-loci are first

calculated from the characteristic equation:  $\det(\lambda I_{2 \times 2} - Z_{eq}^S Y_{eq}^L) = 0$ , and then stability is assessed according to the generalized Nyquist criterion [32].

In what follows, two asymmetric conditions:  $k_z = 0.5$  and  $k_z = 0.1$  are considered for stability assessment, the Nyquist plots are plotted and compared in Fig. 7 (a). It is seen that the Nyquist plots with a small  $k_z$  (i.e.  $k_z = 0.1$ ) indicate a stable system, whereas the ones with a larger  $k_z$  (i.e.  $k_z = 0.5$ ) conclude a marginally unstable system. In Fig. 7 (b), time-domain simulations under these two cases are shown respectively, where small-signal dynamics are invoked by changing the PLL bandwidth at 2s. It is identified that the case with  $k_z = 0.1$  is stable, whereas the one with  $k_z = 0.5$  is unstable, proving the stability results of the Nyquist-based analyses are correct.



(a) Nyquist plots ( $I_{c00} = 0.5$  p.u. CC = 200 Hz, PLL = 40 Hz, SCR = 4)



(b) Time domain simulations (at 2s PLL is changed from 20 to 40 Hz)  
Fig. 7 Nyquist-based stability analysis and verification in simulations

For further model validation, particularly the accuracy on marginally stable/unstable states predictions (i.e. the critical condition), experiments on a downscaled grid-tied VSC system are conducted. The experimental system setup is illustrated in Fig. 8 (a) and (b), and the main circuit parameters of the experimental system are listed in Table IV.

Table IV Main circuit parameters of the experimental system

Name	value	Name	value
$S_n$	3.3. kVA	$L_f$	1.2 mH
$U_n$	155.5 V (peak)	$L_g$	Case1: A,B,C :6mH, 6mH, 2.4mH Case2: A,B,C :8mH, 8mH, 2.0mH
$I_n$	15 A (peak)	$k_z$	Case 1: 0.4 Case 2: 0.25
$f_{sw}$	10 kHz		

> REPLACE THIS LINE WITH YOUR PAPER IDENTIFICATION NUMBER (DOUBLE-CLICK HERE TO EDIT) < 10

To fulfill this target, the control parameters from the Nyquist based-analysis and the experiments at which the critical condition occurs will be compared. In which, the theoretical control parameters of the critical condition are first calculated, denoted as the “theoretical results”. A brief illustration of this process is shown in Fig. 8 (c). It is seen that the critical control parameters are detected by iteratively calling the Nyquist-based stability tests, and checking if it is approaching  $(-1,0 j)$ . Also,

notice that the steady-state operating points are updated once a large change of control parameters is recorded. Once the critical parameters are obtained, they will serve as the reference for the experiments, however, with some modifications until the critical oscillation of the experimental system occurs, the resulting parameters are then denoted as the “experimental results”.

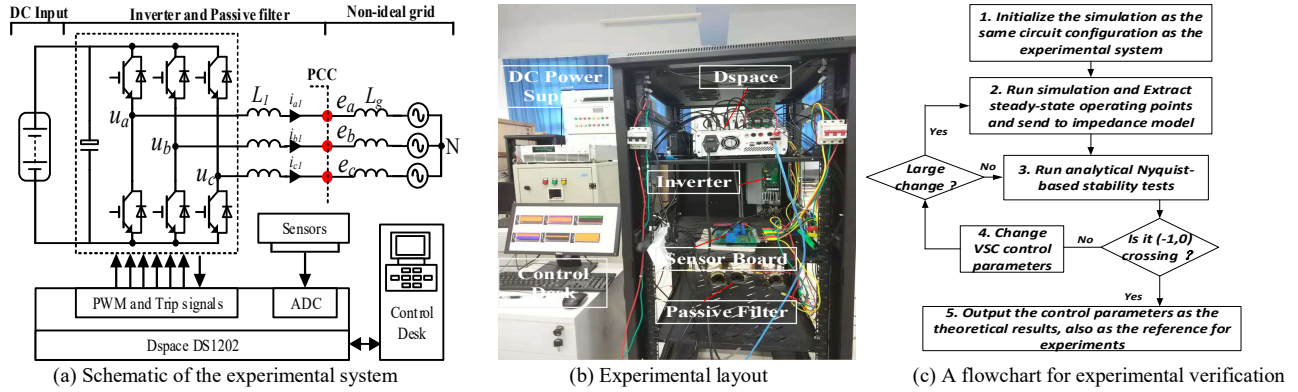


Fig. 8 Experimental system setup and verification method

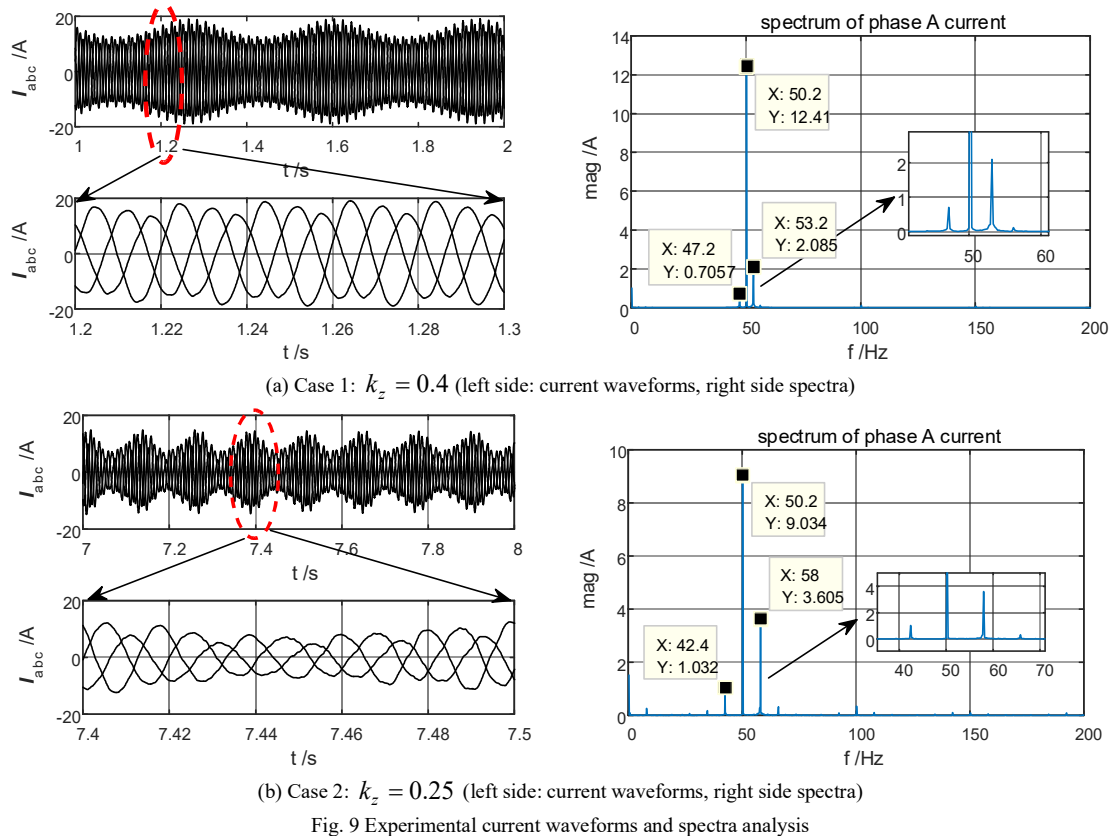


Fig. 9 Experimental current waveforms and spectra analysis

Based on this method, two sets of critical control parameters under  $k_z = 0.4$  (i.e. Case1) and  $k_z = 0.25$  (i.e. Case2) conditions are compared in Table V. It is seen that, though the theoretical and experimental results are not perfectly consistent, in general, the discrepancies are small and satisfactory.

Further, Fig. 9 shows the current waveforms and spectra in accordance with the aforementioned analysis of the critical

stability condition. From the current spectra, one may clearly observe that the mirror 1<sup>st</sup> MFC effect is evident for both cases, whereas the 2<sup>nd</sup> MFC effects are almost invisible. This finding justifies the FCC assumption is feasible for control-related stability analysis. Besides, other frequency components except those related to MFC are also captured in Case 2. They are existent mainly because the oscillating waveforms create quasi-

steady periodical operating points at  $\pm f_{osc} + f_1, f_{osc} = 8\text{Hz}$ , and these new components will interact with the fundamental and the switching frequency, resulting in infinite many frequency couplings, typically they are small and of high orders [30].

Table V Comparison of the experimental and theoretical results

Case	Control parameters		Oscillation frequency	
	Experiment	Theory	Experiment	Theory
Case 1	CC: $k_p=0.4$ , $k_i=40$	CC: $k_p=0.43$ , $k_i=38$	3.2 Hz	2.9 Hz
	PLL: $k_p=0.129$ , $k_i=1.29$	PLL: $k_p=0.129$ , $k_i=1.29$		
	CC: $k_p=0.53$ , $k_i=150$	CC: $k_p=0.6$ , $k_i=160$		
Case 2	PLL: $k_p=0.25$ , $k_i=5.15$	PLL: $k_p=0.25$ , $k_i=5.15$	8.0 Hz	8.4 Hz
	CC: $k_p=0.53$ , $k_i=150$	CC: $k_p=0.6$ , $k_i=160$		
	PLL: $k_p=0.25$ , $k_i=5.15$	PLL: $k_p=0.25$ , $k_i=5.15$		

In overall, the Nyquist-based analysis and verification show that the proposed model is effective for asymmetric ac grid stability analysis. This justifies a former remark that the off-diagonals of the equivalent source model have negligible effects on stability. By comparing those stability cases, another interesting observation that can be found is that it seems the system exhibits a greater capability of maintaining stability if the grid is more asymmetric. A qualitative but straightforward understanding of this finding from the Grid-FCC model is that a “strong grid effect” is captured as  $k_z$  reduces. More analysis on stability, along with a clarification on the feasibility of symmetric models for asymmetric ac grid analysis will be discussed in the next section.

## V. DISCUSSIONS ON THE GRID VOLTAGE ASYMMETRY AND THE FEASIBILITY AND PERFORMANCE OF SYMMETRIC MODELS

Previously, the “grid asymmetry” is primarily defined as the imbalance among three-phase grid impedances. Additionally, grid voltage unbalance is also a sort of grid asymmetry. Hence, it is interesting to see the performance of the proposed model under such conditions. On the other hand, from foregoing analysis, the FCC model is essentially an expansion of the (modified) sequence domain model (i.e. the symmetric model). Hence, it is worthful to clarify the feasibility of the symmetric models for asymmetric ac grid stability analysis.

### A. Impacts of the grid voltage imbalances

In the first place, the grid-voltage asymmetry is defined as the ratio:  $k_g = |U_N / U_P|$ , where  $U_N$  and  $U_P$  are the negative and positive sequence voltage respectively. A comparative study of a small and large grid-voltage asymmetry is shown in Fig. 10, where the “sim 1” denotes the large one (i.e.  $k_g=0.15$ ), and “sim 2” denotes the small one (i.e.  $k_g=0.07$ ).

It is identified that the analytical models are still accurate under such conditions (except the negligible mismatches on the off-diagonals of the equivalent source model), which means the proposed model can capture the major effects of grid asymmetries regardless of the sources (e.g. either three-phase impedance or voltage imbalances). Besides, it is also observed that the extent of grid-voltage asymmetry only has a small impact on the impedance characteristics (see the comparison

between  $k_g=0.15$  and  $k_g=0.07$ ), mainly due to the change of operating points.

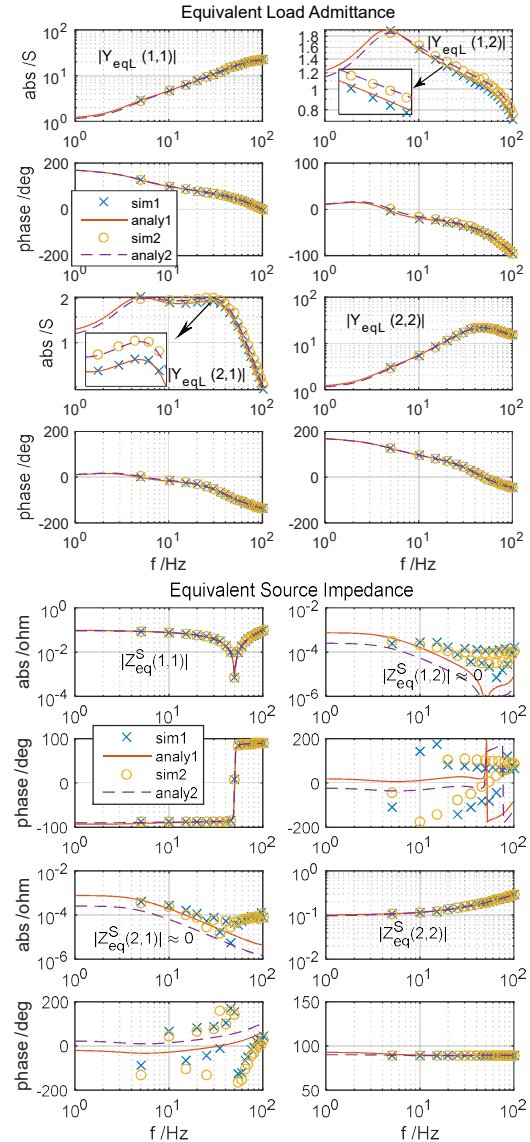


Fig. 10 Impedance validation with grid voltage asymmetry ( $I_{cd0} = 0.5$  p.u., SCR = 2, CC = 300 Hz, PLL = 20 Hz,  $k_z = 0.5$ )

### B. Symmetric models for asymmetric grid stability analysis

In this section, two types of symmetric models will be introduced, and they are compared with the asymmetric model (i.e. the equivalent source and load model) in terms of Nyquist plots and stability margin. First, the *typical symmetric* model is introduced and defined as:  $\mathbf{Y}_{\text{sym\_typ}}^L = \mathbf{Y}_{\text{cPP}}^{\text{hff}}$  and  $\mathbf{Z}_{\text{sym\_typ}}^S = \text{diag}(Z_g(s - j\omega_1), Z_g(s + j\omega_1))$ . However, this model is too simplified since all the asymmetry effects are ignored. A simple improvement can be done by multiplying  $\mathbf{Z}_{\text{sym\_typ}}^S$  with the factor  $k_1$ , from which a *modified symmetric* source model is obtained:  $\mathbf{Z}_{\text{sym\_mod}}^S = k_1 \mathbf{Z}_{\text{sym\_typ}}^S = \mathbf{Z}_{\text{gPP}}^{\text{hff}}$ , and the modified symmetric load model is unchanged, which is

> REPLACE THIS LINE WITH YOUR PAPER IDENTIFICATION NUMBER (DOUBLE-CLICK HERE TO EDIT) < 12

$Y_{sym\_typ}^L$ . It is easily validated that the loop gains of the typical and modified symmetric model have this relationship:  
 $k_1 L_{sym\_typ}(s) = k_1 Z_{gPP}^{hlf} Y_{cPP}^{hlf}(s) = L_{sym\_mod}(s)$ .

First, in Fig. 11, a comparative study in terms of Nyquist plots is presented (only the dominant eigen-loci are shown). It is seen that the typical symmetric model (i.e.  $L_{sym\_typ}(s)$ ) is valid only if  $k_z$  is large (i.e. a small extent of grid asymmetry). As the grid becomes more asymmetric (e.g.  $k_z = 0.5$ ), evident discrepancies between the typical symmetric and the asymmetric model are shown. As a result, in general, this model is not suitable for asymmetric ac grid stability analysis.

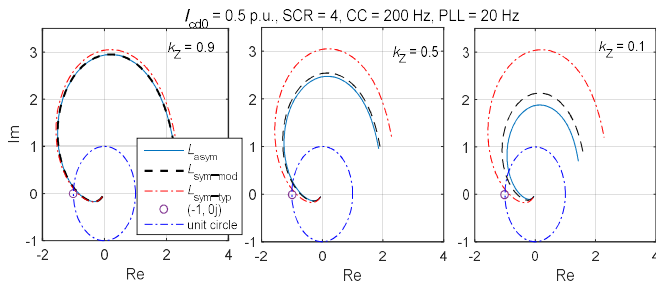


Fig. 11 Nyquist plots comparisons of the symmetric and asymmetric models

The modified symmetric model (i.e.  $L_{sym\_mod}(s)$ ) indeed improves the accuracy to a certain level, the evident error only presents at which the grid asymmetric is severe (e.g.  $k_z < 0.5$ ). Therefore, this model is valid for a certain range of grid asymmetry. On the other hand, the discrepancy between  $L_{sym\_mod}(s)$  and  $L_{asym}(s)$  also implies that the SDC effect cannot be overlooked if grid asymmetry is large.

Based on the Nyquist plots comparison, it is known that both the typical and the modified symmetric model are conservative in terms of stability, particularly the former one. To check if this pessimism holds for a certain range of parameter change, phase margins are evaluated from the Nyquist plots. As a result, a full picture of the stability trends regarding various system configurations is acquired.

In Fig. 12, for a small grid asymmetry (i.e.  $k_z = 0.9$ ), both the typical symmetric and the modified symmetric model are very close to the asymmetric model in terms of stability margin and

trend, particularly the modified symmetric model. However, as the grid asymmetry enlarges (see the comparison under  $k_z = 0.5$  and  $k_z = 0.1$ ), the typical symmetric model exhibits evident error on the stability margins, and generally lower than the prediction of the asymmetric model. As for the modified symmetric model, this pessimism on stability margin still holds, however, the accuracy (i.e. the extent of pessimism) is improved.

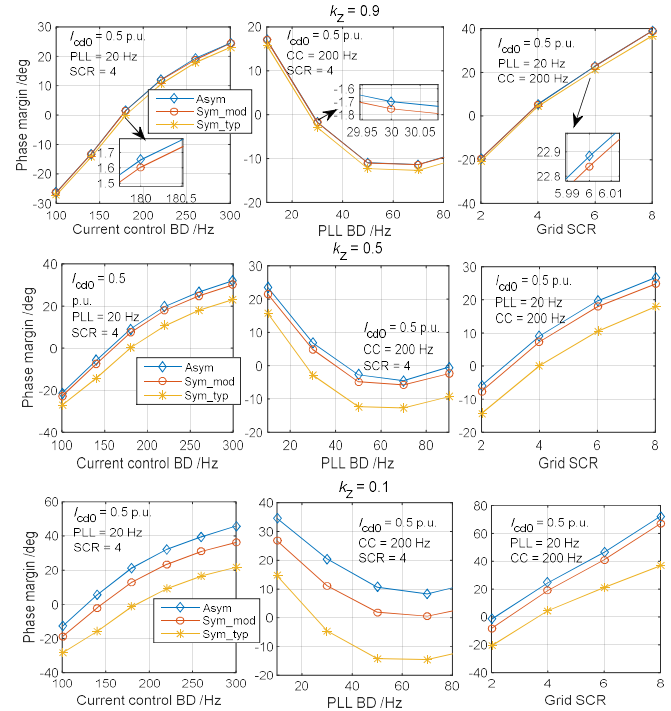


Fig. 12 Analysis of the phase margin under various system configurations

In summary, from those comparisons, it is identified that this pessimism on stability holds consistently for a relatively wide range of parameter variation. Therefore, the effective boundaries of the symmetric models for asymmetric ac grid analysis can be roughly obtained, i.e. the typical symmetric model is valid for  $k_z \leq 0.1$ , and the modified symmetric model is valid for  $k_z \leq 0.5$ . Last, Table VI is formulated to summarize this comparative stability analysis of different models.

Table VII. A summary of stability margin and model accuracy analysis

A summary of stability margin analysis				Impacts of the PLL BD			
Impacts of the grid asymmetry				Values	Small	Medium	Large
Values	$k_z = 0.9$	$k_z = 0.5$	$k_z = 0.1$	Stability margin	Large	Small	Medium
Stability margin	Small	Medium	Large	Stability trend	Initially reduces and then increases		
Stability trend	Monotonously increase			Impacts of the Grid SCR			
Impacts of the current control BD				Values	Small	Medium	Large
Values	Small	Medium	Large	Stability margin	Small	Medium	Large
Stability margin	Small	Medium	Large	Stability trend	Monotonously increase		
Stability trend	Monotonously increase			A summary of the feasibility of symmetric models for asymmetric grid stability analysis			
Grid asymmetry (small, medium, large)				$k_z = 0.9$	$k_z = 0.5$	$k_z = 0.1$	
Error in Margin Prediction (compared to asymmetric model)	Typical symmetric model			Small (negative)	Evident (negative)	Large (negative)	
	Modified symmetric model			Negligible (negative)	Small (negative)	Evident (negative)	
Remark	The typical symmetric model is not suitable for asymmetric ac grid stability analysis The modified symmetric model is valid for a certain range of grid asymmetry, overall, the stability predications are over-pessimistic.						

## VI. CONCLUSIONS

This work developed an analytical impedance model of an unbalanced grid-VSC system for asymmetric ac grids stability analysis. The proposed models have a clear physical interpretation in frequency-domain, reflecting the interactions between the VSC controls (i.e. MFC effect) and the asymmetric ac grid (i.e. SDC effect). The proposed model is thoroughly validated within the frequency range of interest (i.e. the FCC related to control dynamics), whereas the high-frequency range outside this scope is not modeled (e.g. switching and digital delays). Therefore, in theory, the harmonic unstable phenomenon characterized as high-frequency dynamics may not be effectively justified by this model, which are worth being explored in future studies.

On the other hand, several significant concerns on the stability and the feasibility of symmetric models for asymmetric grid analysis are discussed and clarified. It turns out that the typical symmetric model is not suitable for asymmetric grid stability analysis, whereas the modified typical model has some improvements but still only valid for a certain range of grid asymmetry. Overall, they are over-pessimistic on stability assessments. Another finding from the stability analysis could be interesting is that the grid-VSC system exhibits a greater capability of maintaining stability if the grid asymmetry is more severe.

## ACKNOWLEDGMENT

Gratitude goes to Dr. Ning Gao, Department of Electrical Engineering, Shanghai Maritime University, and Mr. Haoshu Shao, Department of Electrical Engineering, Shanghai Jiao Tong University, for the support and help with experimental works.

## REFERENCES

- [1] Teodorescu R, Liserre M, Rodriguez P. "Introduction," in Grid converters for photovoltaic and wind power systems. Chichester, United Kingdom: John Wiley & Sons, 2011, pp:1-4.
- [2] Flourentzou N, Agelidis V G, Demetriades G D. "VSC-Based HVDC Power Transmission Systems: An Overview," IEEE Trans. Power Electron, vol.24, no.3, pp.592-602, 2009.
- [3] C. Zhang, X. Cai, Z. Li, A. Rygg and M. Molinas, "Properties and physical interpretation of the dynamic interactions between voltage source converters and grid: electrical oscillation and its stability control," in IET Power Electronics, vol. 10, no. 8, pp. 894-902, 6 30 2017.
- [4] Liu, H., Xie, X., He, J., Xu, T., Yu, Z., Wang, C., & Zhang, C. (2017). Subsynchronous interaction between direct-drive PMSG based wind farms and weak AC networks. IEEE Transactions on Power Systems, 32(6), 4708-4720.
- [5] C. Li, "Unstable Operation of Photovoltaic Inverter from Field Experiences," IEEE Trans. Power Del, to be published.
- [6] M. Raza, E. Prieto-Araujo and O. Gomis-Bellmunt, "Small-Signal Stability Analysis of Offshore AC Network Having Multiple VSC-HVDC Systems," in IEEE Transactions on Power Delivery, vol. 33, no. 2, pp. 830-839, April 2018.
- [7] K. M. Alawasa, Y. A. R. I. Mohamed and W. Xu, "Active Mitigation of Subsynchronous Interactions Between PWM Voltage-Source Converters and Power Networks," in IEEE Transactions on Power Electronics, vol. 29, no. 1, pp. 121-134, Jan. 2014.
- [8] L. P. Kunjumammed, B. C. Pal, C Oates, and K.J. Dyke, "Electrical Oscillations in Wind Farm Systems: Analysis and Insight Based on Detailed Modeling," IEEE Trans. Sustainable Energy, vol. 7, no. 1, pp. 1-12, 2015.
- [9] X. Wang and F. Blaabjerg, "Harmonic Stability in Power Electronic Based Power Systems: Concept, Modeling, and Analysis," in IEEE Transactions on Smart Grid, 2018 (online).
- [10] Belkhat M, "Stability criteria for AC power systems with regulated loads," Ph.D. dissertation, Purdue University, USA, 1997.
- [11] B. Wen, D. Boroyevich, R. Burgos, P. Mattavelli and Z. Shen, "Small-Signal Stability Analysis of Three-Phase AC Systems in the Presence of Constant Power Loads Based on Measured d-q Frame Impedances," in IEEE Transactions on Power Electronics, vol. 30, no. 10, pp. 5952-5963, Oct. 2015.
- [12] L. Harnefors, M. Bongiorno and S. Lundberg, "Input-Admittance Calculation and Shaping for Controlled Voltage-Source Converters," in IEEE Transactions on Industrial Electronics, vol. 54, no. 6, pp. 3323-3334, Dec. 2007.
- [13] J. Sun, "Small-Signal Methods for AC Distributed Power Systems—A Review," in IEEE ESTS., Baltimore, Maryland, pp. 44-52, 2009
- [14] M. K. Bakhshizadeh, X. Wang, F. Blaabjerg, J. Hjerrild, L. Kocewiak, C. L. Bak, and B. Hesselbæk, "Couplings in Phase Domain Impedance Modeling of Grid-Connected Converters," IEEE Trans. Power Electron, vol. 31, no. 10, pp. 6792-6796, 2016.
- [15] M. Céspedes and J. Sun, "Impedance Modeling and Analysis of Grid-Connected Voltage-Source Converters," in IEEE Transactions on Power Electronics, vol. 29, no. 3, pp. 1254-1261, March 2014.
- [16] X. Wang, L. Harnefors, F. Blaabjerg, and P.C. Loh, "A Unified Impedance Model of Voltage-Source Converters with Phase-Locked Loop Effect," IEEE ECCE, United States, pp. 1-8, 2016.
- [17] L. Harnefors, "Modeling of Three-Phase Dynamic Systems Using Complex Transfer Functions and Transfer Matrices," IEEE Trans. Ind. Electron, vol. 54, no. 4, pp. 2239-2248, 2007
- [18] A. Rygg, M. Molinas, C. Zhang and X. Cai, "A Modified Sequence-Domain Impedance Definition and Its Equivalence to the dq-Domain Impedance Definition for the Stability Analysis of AC Power Electronic Systems," in IEEE Journal of Emerging and Selected Topics in Power Electronics, vol. 4, no. 4, pp. 1383-1396, Dec. 2016
- [19] C. Zhang, X. Cai, A. Rygg and M. Molinas, "Sequence Domain SISO Equivalent Models of a Grid-Tied Voltage Source Converter System for Small-Signal Stability Analysis," in IEEE Transactions on Energy Conversion, vol. 33, no. 2, pp. 741-749, June 2018.
- [20] S. Shah and L. Parsa, "Impedance Modeling of Three-Phase Voltage Source Converters in DQ, Sequence, and Phasor Domains," in IEEE Transactions on Energy Conversion, vol. 32, no. 3, pp. 1139-1150, Sept. 2017.
- [21] Wereley, N. M.. Analysis and control of linear periodically time varying systems, Diss. Massachusetts Institute of Technology, 1990.
- [22] Vanassche, P., Gielen, G., & Sansen, W. M. Systematic modeling and analysis of telecom frontends and their building blocks. Springer Science & Business Media, 2006.
- [23] J. Kwon, X. Wang, F. Blaabjerg, C. L. Bak, V. S. Sularea and C. Busca, "Harmonic Interaction Analysis in a Grid-Connected Converter Using Harmonic State-Space (HSS) Modeling," in IEEE Transactions on Power Electronics, vol. 32, no. 9, pp. 6823-6835, Sept. 2017.
- [24] J. Kwon, X. Wang, F. Blaabjerg, C. L. Bak, A. R. Wood and N. R. Watson, "Linearized Modeling Methods of AC-DC Converters for an Accurate Frequency Response," in IEEE Journal of Emerging and Selected Topics in Power Electronics, vol. 5, no. 4, pp. 1526-1541, Dec. 2017.
- [25] J. Lyu, X. Cai, M. Amin and M. Molinas, "Sub-synchronous oscillation mechanism and its suppression in MMC-based HVDC connected wind farms," in IET Generation, Transmission & Distribution, vol. 12, no. 4, pp. 1021-1029, 2 27 2018.
- [26] E. Möllerstedt, "Dynamic analysis of harmonics in electrical systems," Ph.D. dissertation, Lund University, Sweden, 2000.
- [27] H. Nian, L. Chen, Y. Xu, H. Huang and J. Ma, "Sequences Domain Impedance Modeling of Three-Phase Grid-Connected Converter Using Harmonic Transfer Matrices," in IEEE Transactions on Energy Conversion, vol. 33, no. 2, pp. 627-638, June 2018.
- [28] M. K. Bakhshizadeh, F. Blaabjerg, J. Hjerrild, X. Wang, L. Kocewiak and C. L. Bak, "A Numerical Matrix-Based Method for Stability and Power Quality Studies Based on Harmonic Transfer Functions," in IEEE Journal of Emerging and Selected Topics in Power Electronics, vol. 5, no. 4, pp. 1542-1552, Dec. 2017.

- [29] G. C. Paap, "Symmetrical components in the time domain and their application to power network calculations," in *IEEE Transactions on Power Systems*, vol. 15, no. 2, pp. 522-528, May 2000.
- [30] J. Sun and H. Liu, "Sequence Impedance Modeling of Modular Multilevel Converters," in *IEEE Journal of Emerging and Selected Topics in Power Electronics*, vol. 5, no. 4, pp. 1427-1443, Dec. 2017.
- [31] J. Sun, "Impedance-Based Stability Criterion for Grid-Connected Inverters," in *IEEE Transactions on Power Electronics*, vol. 26, no. 11, pp. 3075-3078, Nov. 2011.
- [32] B. Wen, D. Boroyevich, R. Burgos, P. Mattavelli and Z. Shen, "Inverse Nyquist Stability Criterion for Grid-Tied Inverters," in *IEEE Transactions on Power Electronics*, vol. 32, no. 2, pp. 1548-1556, Feb. 2017.



**Chen Zhang** received the B.Eng. degree from the China University of Mining and Technology, China, and the Ph.D. from Shanghai Jiao Tong University, China, in 2011 and 2018 respectively. He was a Ph.D. Visiting Scholar with the Department of Engineering Cybernetics, Norwegian University of Science and Technology (NTNU), Norway, in 2015. Currently, he is a Postdoctoral Research Fellow at NTNU. His research interest is modeling and stability analysis of VSCs-based energy conversion systems, where the aim is to reveal the fundamental dynamics and stability mechanisms behind the grid-tied VSCs.



**Marta Molinas** (M'94) received the Diploma degree in electromechanical engineering from the National University of Asuncion, Asuncion, Paraguay, in 1992; the Master of Engineering degree from Ryukyu University, Japan, in 1997; and the Doctor of Engineering degree from the Tokyo Institute of Technology, Tokyo, Japan, in 2000. She was a Guest Researcher with the University of Padova, Padova, Italy, during 1998. From 2004 to 2007, she was a Postdoctoral Researcher with the Norwegian University of Science and Technology (NTNU) and from 2008-2014 she has been professor at the Department of Electric Power Engineering at the same university. She is currently Professor at the Department of Engineering Cybernetics, NTNU. Her research interests include stability of power electronics systems, harmonics, instantaneous frequency, and non-stationary signals from the human and the machine. She is Associate Editor for the *IEEE Journal JESTPE*, *IEEE PELS Transactions* and Editor of the *IEEE Transactions on Energy Conversion*. Dr. Molinas has been an AdCom Member of the IEEE Power Electronics Society from 2009 to 2011.



**Atle Rygg** received the MSc degree in Electrical Engineering from the Norwegian University of Science and Technology (NTNU) in 2011. From 2011 to 2015 he was a research scientist at SINTEF Energy Research in the field of power electronics. He received his Ph.D. at department of engineering cybernetics at NTNU, 2018. His topic or research is impedance-based stability analysis of power electronic

systems, where the aim is to contribute to the fundamental understanding in this family of methods.



**Jing Lyu** (S'14-M'16) received the B.Eng. degree from China University of Mining and Technology, Jiangsu, China, in 2009, the M.Eng. and Ph.D. degrees from Shanghai Jiao Tong University, Shanghai, China, in 2011 and 2016, respectively, all in electrical engineering. He was a Postdoctoral Research Fellow with the Department of Engineering Cybernetics, Norwegian University of Science and Technology, Trondheim, Norway, from 2016 to 2017. Since 2018, he has been a tenure-track Assistant Professor with the Department of Electrical Engineering, Shanghai Jiao Tong University. His current research interests include dynamic stability of MMC-based HVDC connected wind farms/PV plants, modeling and control of modular multilevel converter, dynamic modeling of wind turbines and wind farms, and impedance modeling.



**Xu Cai** received the B.Eng. degree from Southeast University, Nanjing, China, in 1983, and the M.Sc. and Ph.D. degrees from the China University of Mining and Technology, Xuzhou, China, in 1988 and 2000, respectively. He was with the Department of Electrical Engineering, China University of Mining and Technology, as an Associate Professor from 1989 to 2001. He was the Vice Director of the State Energy Smart Grid R&D Center, Shanghai, China, from 2010 to 2013. He has been with Shanghai Jiao Tong University, Shanghai, as a Professor since 2002, where he has also been the Director of the Wind Power Research Center since 2008. His current research interests include power electronics and renewable energy exploitation and utilization, including wind power converters, wind turbine control system, large power battery storage systems, clustering of wind farms and its control system, and grid integration.